

Infrared actuation in aligned polymer-nanotube composites

S. V. Ahir, A.M. Squires, A.R. Tajbakhsh and E.M. Terentjev

Cavendish Laboratory, University of Cambridge, J.J. Thomson Avenue, Cambridge CB3 OHE, U.K.

Rubber composites containing multi-walled carbon nanotubes have been irradiated with near infrared light to study their reversible photo-mechanical actuation response. We demonstrate that the actuation is reproducible across differing polymer systems. The response is directly related to the degree of uniaxial alignment of the nanotubes in the matrix, contracting the samples along the alignment axis. The actuation stroke depends on the specific polymer being tested, however, the general response is universal for all composites tested. We conduct a detailed study of tube alignment induced by stress and propose a model for the reversible actuation behavior, based on the orientational averaging of the local response. The single phenomenological parameter of this model describes the response of an individual tube to adsorption of low-energy photons; its experimentally determined value may suggest some ideas about such a response.

PACS numbers: 42.70.Gi, 71.35.Gg, 73.22.Lp, 81.07.-b, 82.35.Np

I. INTRODUCTION

Many structures are able to change their mechanical properties and dimensions when an appropriate stimulus is applied. This phenomenon is commonly called actuation. The energy from an external source triggers changes in the internal state of the system, leading to a mechanical response much larger than the initial input. This ability to unlock internal work in a solid state structure is of key importance for many actuator applications. Actuators with differing characteristics and mechanisms have been widely adopted by industry to fill a variety of technological requirements [1] with some having a one-way response, while others providing an equilibrium, reversible response to the given stimulus. Shape-memory alloys [2] or polymers [3] are good examples of such smart actuating systems. However, in most cases a shape memory system works only in one direction, requiring a reset after the actuation. Only very few systems can reversibly actuate and then return back to the equilibrium shape once the stimulus is removed. So far only liquid crystal elastomers [4] have proven to be a truly equilibrium reversible actuating system.

A polymer benign to external stimulus can also be made to actuate when blended with one or more distinctly different materials to impart a new physical response leading to the actuation process. A recent article has demonstrated one such system, based on a common silicon rubber filled with a low concentration of aligned carbon nanotubes, actuating in response to infrared radiation [5]. Apart from actuation itself, the stimulation of functionalized nanotubes by infrared (IR) radiation is also proving an effective technique, e.g. in biomedical applications [6]. Clearly, there are rich prospects and much motivation to understand nanotube action and the actuation behavior under IR irradiation when they are embedded in a polymer matrix.

The work presented here focuses on the use of multi-walled carbon nanotubes (MWCNTs) to impart equilibrium mechanical actuation in the rubbery matrix. The properties of multi-walled nanotubes has been well

documented for over a decade [7, 8, 9]. Their behavior in polymer composites is less well understood but some reviews have recently appeared in the literature [10, 11, 12, 13, 14]. For mechanical applications, the interface between the tube surface and the host polymer is of critical importance and most of the studies have focussed on this aspect. In contrast, the nature of the active response of nanotubes within a polymeric matrix has yet to be fully understood. The complex behavior of tubes is often simplified and analogies are made with aligned rigid rods. It is unclear whether such analogies are always valid, especially when the tubes do not necessarily form rigid rods in a polymer matrix and certainly do not align unless an external field is present [14].

The actuating properties of MWCNTs have recently been elucidated upon with the possibility of designing nanoelectromechanical (NEMS) systems [15]. The actuator properties of individual bending MWCNTs under an applied electric field have been studied experimentally [16]. The torsional actuation behavior of multi-walled tubes has also been reported [17, 18]. These works are important but we note that all these studies focus on individual tubes and not a collection of tubes, nor their properties within a continuous elastic matrix. The massive elastic response of single-walled nanotube bundles, when stimulated by light, was very effectively demonstrated by Zhang and Iijima [19], although little work has followed from their discovery. They showed the bundles responding to visible light and a near IR laser radiation by elastically changing their dimensions; examining the figures in [19] we deduce that the induced strain must be about 20%. In the context of this paper, we shall refer to the actuation stroke as the change in strain, when an external stimulus is applied.

There are several reports of actuation behavior of polymer-nanotube composites [20, 21, 22]. These works have focussed on accentuating the already present features of the host matrix by adding nanotubes. The tubes act to exaggerate the response by either improving electromechanical properties or increasing heat transfer efficiency due to the inherent high conductivity [14, 23]

that originates from their delocalized π -bonded skeleton. Recent work has departed from this traditional ‘improvement’ scheme and asked whether it is possible to blend nanotubes with benign polymers to create new composite actuator properties, that otherwise would not occur in that system. Such effects have been observed by Courty *et al.* [24] where electric field stimulation of liquid crystal elastomers with embedded MWCNTs lead to mechanical contraction.

Similarly, the photomechanical response from MWCNTs when embedded in a silicone rubber (PDMS) matrix [5] is a new effect. The pristine elastomer shows no response to near IR radiation, yet the presence of nanotubes causes a strong reversible response that can be tailored by manipulating the degree of alignment the tubes experience. The present work expands on such a simple polymer nanocomposite system and goes on to show that the effect can exist independently of the host polymer matrix which, by the presence of MWCNTs, produces a mechanical response to the IR irradiation. We show that both a compression and an extension response can be achieved (depending on the external uniaxial strain applied to the composite sample), but that the magnitude of the actuation stroke strongly depends on the host polymer used. We also develop a simple model that considers the orientational ordering of nanotubes in the matrix along with their individual and bulk actuating behavior.

This paper is organized as following: after giving details of preparation and basic composite characterization, we concentrate on the analysis of tube orientation induced by stretching of the host polymer matrix, section III. We then turn to the IR-stimulated actuation, section IV, and study different nanocomposite systems in some detail (although the majority of our studies remain on the PDMS system). Section V presents a simple theoretical model that might well describe the actuation mechanism and compares it with our experimental data and the literature. We conclude that two-way actuation behavior is dependent on nanotube orientation, but is independent of the chosen homogenous polymer matrix and can occur in any rubbery solid, albeit with varying magnitude. It is thought that no other materials of any class (metal, polymer, ceramic) can display this behavior and to such large effect, thus, the study of the underlying physics of such systems is of clear scientific, medical and commercial importance.

II. EXPERIMENTAL

A. Materials

There are many different sources of carbon nanotubes on the market today. After extensive searching and testing, we have settled on nanotubes provided by Nanosstructured & Amorphous Materials, Inc. (USA). These are multi-walled, with the core diameter between 5-10nm, outer diameter of 60-100nm and length between 5-15 mi-

crons. Purity has been verified (with SEM) as >95% in raw form from the supplier, in agreement with specification. These nanotubes were not surface-modified at any time during processing and are used throughout this study for all polymers tested. Chemical functionalization is necessary in many nanocomposite fields, but in our work it has been avoided to reduce the number of variables in the system. We share the views of other authors that chemical functionalization of the tube walls will degrade the properties of the tubes overall due to further introduction of sp^3 hybridized carbon defects [25, 26].

Three types of polymer have been tested; PDMS rubber (crosslinked polydimethylsiloxane), SIS (styrene-isoprene-styrene) triblock thermoplastic elastomer and a nematic liquid crystal elastomer (LCE, in both mono and polydomain form). Each type of polymer has a unique preparation method outlined in the following sections. Where possible, similarities in processing have been kept. Table I lists the composites made and their abbreviations.

1. PDMS composite preparation

The PDMS (Sylgard 184TM) silicone elastomer system was obtained from Dow Corning, USA, in the form of the main compound and the hydrosilane curing agent (crosslinker). In pristine conditions, the mixing and crosslinking procedure gives a uniform solvent-free elastomer. We have verified (with SEM on cryo-microtomed and freeze-fractured surfaces) that the resulting polymer network is pure crosslinked PDMS with no filler particles, as sometimes is the case with supplied elastomer mixes.

The nanotube-polymer composite was fabricated by first carefully weighing the desired quantity of nanotubes and the polymer compound. Calculations of weight percentage take into account the weight of crosslinker, to be later used in the mixture. The highly viscous fluid was sheared using an Ika Labortechnik mixer for a minimum of 24 hours.

The crosslinker was added to the mixture after 24

TABLE I: List of host polymer materials, nanotube loading and the abbreviations of resulting composites.

Host	Tube loading (wt%)	Abbreviation
PDMS	0, 0.02, 0.3, 0.5, 1, 2, 3, 4 & 7	PDMS, PDMS0.02, PDMS0.3, PDMS0.5, PDMS1 .. & PDMS7
Mono LCE	0 & 0.2	MLCE & MLCE0.2
Poly LCE	0 & 0.15	PLCE & PLCE0.15
SIS	0.01	SIS0.01

hours. The ratio of crosslinker to PDMS was 1:10, according to Sylgard 184TM specification, ensuring negligible sol fraction after preparation of the pristine network. The sample was then further sheared for another 30 seconds before being placed in vacuum for 5 minutes to degas, at all times remaining at ambient temperature to ensure little crosslinking reaction takes place in this time. After removing the air cavities, that unavoidably form during shear mixing, the mixture was deposited in a specially designed reactor (centrifuge compartment with PTFE film lining its inner wall) and placed in a centrifuge at 5000rpm and 80°C. At this temperature the PDMS crosslinking is much faster and the centrifugation achieves the uniform thickness and full homogenization of resulting rubber composite samples.

The subsequent processing depends on the target sample properties. If we require a completely non-aligned nanotube dispersion, the sample remains in the reactor for 24 hours, resulting in a homogeneous elastomer composite. In some cases (as will be clear from the text below) we aim to produce a sample with nanotubes permanently pre-aligned. In this case the initial mix remains in the reactor, at 80°C, for 14 minutes (calculated from separate measurements of crosslinking reaction rates). The partially crosslinked network was then removed from the reactor and aligned mechanically by applying uniaxial extension using specially designed clamps. Removing the sample from the reactor after what is a relatively short period of time ensures that it is being mechanically aligned while still having over 50% of crosslinking to take place. Finally, while still constrained in the clamps, the sample was placed in an oven at 70°C for a further 24 hours as it finished its crosslinking cycle under stress. As a result a homogeneous elastomer was prepared where the nanotubes had a preferred orientation induced by the processing technique and are also well dispersed in the matrix. The degree of nanotube alignment in each sample was quantified using X-ray techniques (discussed below).

There is a separate question of solvent and shearing conditions, and the time required for the full MWCNT dispersion; systematic studies of nanotube dispersion and re-aggregation rates are to be published shortly. The quality of nanotube dispersion is monitored throughout the processing with the use, initially, of optical microscopes and later with a High-Resolution Scanning Electron Microscope (HRSEM, Phillips XL 30 series) as aggregate sizes reduce below optical resolution. We find that a shearing regime of high-viscosity mixture, lasting 24 hours, is suitable in removing nanotube aggregates. Samples are identified by the wt% of MWCNTs mixed with the PDMS and the abbreviations assigned to them in table I. Most experiments have been conducted on the 0, 0.02, 0.3, 0.5, 1, 2, 3, 4 and 7wt% MWCNTs in PDMS elastomer films. A sample with 3wt% carbon black instead of nanotubes has also been made using the same procedure.

2. Nematic elastomer composite preparation

There is a wealth of literature regarding liquid crystal elastomer (LCE) preparation [4]. For our purposes, we have tested two specific types of LCE: polydomain and monodomain, with uniaxially aligned nematic director. Control samples containing no nanotubes were made, following the procedure introduced in [27] and widely used in the field since. The procedure of nanocomposite preparation was detailed in [24]. The polysiloxane backbone chains (\sim 60 monomer units long) had their Si–H bonds reacted, using platinic acid catalyst, with the terminal vinyl groups of the mesogenic rod-like molecule 4-methoxyphenyl)–4'-buteneoxy benzoate (MBB) and the two-functional crosslinker 1,4-di-11-undeceneoxy benzene (11UB), with the molar ratio 18:1 (thus achieving the 9:1 ratio of substituted groups on each chain, or the effective 10% crosslinking density). The crosslinking was initiated by a combination of adding the catalyst and heating to 80°C in the already described centrifugation reaction chamber. The subsequent procedure of two-stage crosslinking, with intermediate stretching to induce director alignment, is similar to the procedure of PDMS alignment above.

Polydomain control samples were made identically with the single exception that no uniaxial extension is applied during the crosslinking cycle. This avoids orientational bias being introduced during processing.

For LCE nanocomposites, a minor modification is made. Before the crosslinker and catalyst were added, MWCNTs were shear mixed into the polymer to ensure homogenous dispersion. Due to the sensitivity of the crosslinker and catalyst, shear mixing is reduced to 4 hours at elevated temperatures (\sim 50°C). This is acceptable as the nanotube concentration in such systems was very small (0.15–0.2wt%) while the nematic polymer is highly viscous. A higher concentration in such a system is currently unachievable due to catalyst and crosslinker sensitivity limitations.

3. SIS composite preparation

The SIS nanocomposite was made by adding the desired quantity of tubes (0.01wt%) to the melt of SIS symmetric triblock copolymer (14% of polystyrene, obtained from Sigma Aldrich) in the presence of small amount of toluene solvent. The solvent dilutes the otherwise rubbery thermoplastic system and allows shear mixing at 40°C for 24 hours. The solvent was added in small portions during the mixing cycle to maintain the mixture in a high-viscosity state. Once the dispersed state was achieved, fibers could be drawn from the mixture and left to air dry. During this period the PS micelles are formed in the usual way [28] to form the elastic network surrounding and encapsulating the nanotubes. We note that too high a loading of MWCNT prevents physical crosslinks from occurring in the host polymer and thus

nanotube content was kept to a very low level.

In all cases the sample dimensions were kept approximately constant, $1.5\text{mm} \times 3\text{cm}$, with thickness 0.2mm .

B. Experimental techniques

The main part of this study, and purpose of this paper, is concerned with the response of these materials to infrared radiation and to that end a specially constructed rig was built to test the actuator response. Two dynamometers were used in this study; a 25g dynamometer for small sensitive measurements and a larger 55g dynamometer allowing a larger range of responses to be tested. The dynamometers (Pioden Systems Ltd) were housed in a custom made thermal-control box with an open front end. The device, together with an independent thermocouple, outputs data via a DAQ card to a PC, see Fig. 1. The sample (S) was clamped in the frame with its length controlled by the micrometer (M), with $\pm 0.001\text{mm}$ accuracy, and the exerted force measured by the dynamometer (D). Thermocouples (T_1 and T_2) were placed in front and behind, on the sample surface. The actuation was induced by the light source (IR), Schott KL1500 LCD, with quoted peak power density at $\approx 675\text{nm}$, $702\ \mu\text{W}/\text{cm}^2$ at 1m distance. The source uniformly illuminated the sample from $\sim 2\text{cm}$ distance. Measuring the scaling of the intensity decay with distance, we obtained that the power density delivered to the sample was $\sim 1.5\text{mW}/\text{cm}^2$ at 675nm . The rig was enclosed in the thermally controlled compartment, and calibrated with weights to give a direct measure of stress and strain.

Figure 2 shows the spectral distribution of the light source, as well as the nanotube absorbance. These measurements were carried out on a Varian Cary 300 BIO UV-visible spectrophotometer in the $190\text{-}1000\text{nm}$ range, adjusted for the background. Absorption units $\text{Au} = \log[I_0/I_{\text{transmitted}}]$ indicate that the PDMS control sample of given thickness transmits $\sim 70\%$ of light across the spectrum. In contrast, the same thickness of low-loading PDMS0.3 composite absorbs $> 97\%$ of light across a range of wavelengths. The strong absorbtion of light by nanotubes is a well-known effect, although the relatively flat spectral distribution was a surprise in our case, Fig. 2.

To standardize the results across all samples, pre-experimental checks were undertaken to accurately find the zero strain value of each experiment. The gradient of the stress-strain curve for a buckled sample was equated with the gradient for the stress-strain curve of the taut sample – the meeting point of the two lines designates the zero-point strain, with the length of sample defined as L_0 . The imposed extensional strain is calculated by $\varepsilon = (L - L_0)/L_0$, with L provided from the micrometer reading.

After a fixed pre-strain was applied to each sample, the stress was allowed to relax for a minimum of 10 minutes.

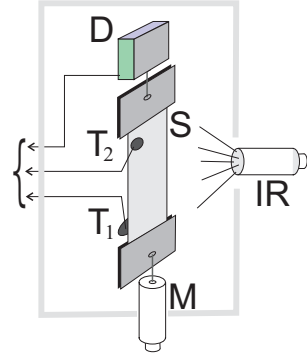


FIG. 1: Scheme of the apparatus; see text for detail.

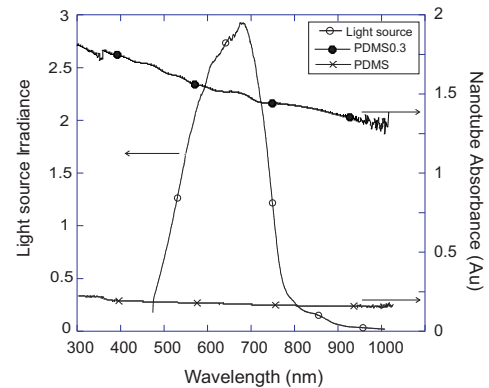


FIG. 2: Spectral data of the light source (left axis, arb. units), and the normalized absorbtion of the PDMS0.3 composite and the control pristine PDMS elastomer (right axis).

After this relaxation period, readings of stress were taken for 1-2 minutes, to verify that the material is equilibrated, and then the IR source was switched on to full intensity. After a period of exposure, the light source was switched off and further relaxation data collected. After completion, the sample was relaxed and then this protocol was repeated for a different applied pre-strain ε . Each sample is tested under a range of applied pre-strains between 2% and 40% ($0.02 \leq \varepsilon \leq 0.4$). In order to avoid a systematic influence of pre-strain, through thermal history and possible degradation, we applied the different values of ε in random order, not sequentially. The LCE composites have been tested for even larger deformation as they can spontaneously undergo thermal strains of hundreds of percent [4].

Our attempts to rationalize the observed response, changing qualitatively on increasing the applied pre-strain, invoke the concept of increasing nanotube alignment under uniaxial deformation. To monitor this, wide angle X-ray diffraction measurements were carried out on a Phillips PW1830 Wide Angle x-ray generator (WAXS) using $\text{Cu}_K\alpha_1$ radiation (1.54\AA), running at 40kV and 40mA. A specially designed clamp was used allowing measurement of the X-ray images as a function of the applied strain during the experiment. Azimuthal scans

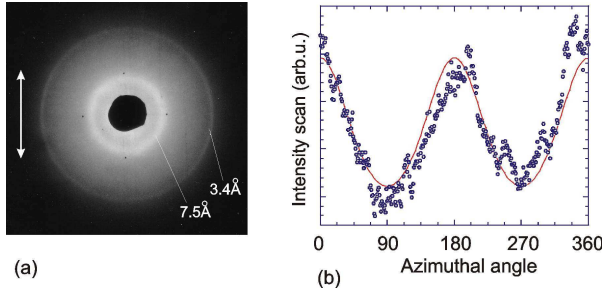


FIG. 3: (a) The X-ray scattering image showing key reflections; the outer ring (3.4\AA) is the signal from the multiwall nanotubes. The inner ring (7.5\AA) represents the PDMS mesh size, see section III B. The arrow shows the direction of the uniaxial aligning strain. (b) The typical azimuthal intensity variation, $I(\beta)$, at a scattering angle of 3.4\AA reflection. The data is fitted by the model [29].

of intensity were generated, Fig. 3, and fitted with theoretical models. The method of background correction employed is crucial. Two to three different regions were selected from an image to gather an average of background noise which is then subtracted from the azimuthal curves generated. This is repeated for all scattering images before order parameter was calculated.

With the IR irradiation, the question always exists, whether the response is due to photon absorption, or the trivial heating of the materials (which does take place during irradiation). The technique used to measure temperature involves two thermocouples and we were reasonably sure that the measured increase in temperature ($\sim 15\text{--}20^\circ\text{C}$) is a true temperature across the sample. A separate study was conducted using thermocouples on the surface and embedded within the sample which showed similar values throughout for any relevant time-scale. The samples were kept purposely thin to ensure very quick heat conduction. To compare the effects, the same experiment was carried out on the PDMS1 sample, with the infrared source replaced by a mica-insulated heater (Minco Products Inc.) mounted approximately 10mm away from the sample. Temperature was regulated through an integrating controller using thermocouples mounted on the sample. The maximum temperature reached was $15\text{--}20^\circ$ above ambient, and although thermo-mechanical response was present, it was much slower and almost an order of magnitude smaller than the direct IR-irradiation effect.

III. MATERIAL CHARACTERIZATION

A. Elastic strength

Figure 4 shows a summary of the linear mechanical response of our nanocomposites for different nanotube loadings in the crosslinked PDMS matrix. As the concentration of MWCNTs is increased the rubbery network

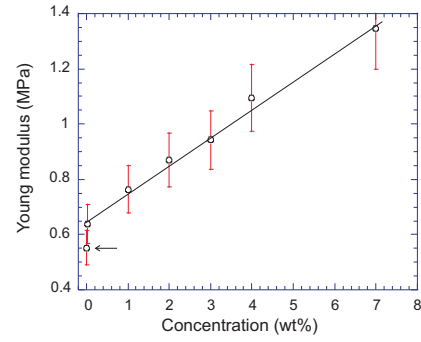


FIG. 4: Young modulus Y for PDMS nanocomposites at increasing MWCNT loading. The arrow points at the value for control PDMS rubber.

becomes stiffer and Young modulus Y (the response to static linear extension) of the composites increases. This is expected and in line with literature findings [12, 30]. An account for subtle variations in measured moduli could be obtained from the analysis of the polymer-nanotube interface and relaxation of local stress in the composites. This is not the focus of the work presented here.

At very low nanotube loading one might expect that large regions of rubbery network are still pristine. However, even with the lowest nanotube loading ($\sim 0.02\text{wt\%}$), a small but significant increase in modulus was observed suggesting that the presence of the tubes even in tiny quantities has an immediate mechanical effect. Starting from $\sim 0.02\text{wt\%}$ the linear increase of the modulus was observed, characteristic of non-interacting inclusions in the elastic matrix. We observe an almost three-fold linear increase in the elastic modulus from 0-7wt%.

It can be argued that at higher loading the concentration dependence must become non-linear, quadratic at first indicating the pair interactions between nanotube inclusions, etc. This may signify the onset of a ‘mechanical’ percolation within the composite system. One may be tempted to make a connection between the onset of this non-linear regime and the separately determined electric percolation threshold, when the composite becomes conducting through nanotube contacts. Unfortunately, it is difficult to make an unambiguous connection in a crosslinked system: an increase in tube concentration would undoubtedly increase the modulus Y – but would also cause a reduction in the crosslinker concentration (the presence of nanotubes has an inhibitive effect on siloxane reactions). Overall, the Young’s modulus of such a nanocomposite would not be able to directly reflect the nanotube interactions.

For completeness, let us quote the measured Young modulus values for the other nanocomposite systems under study – MLCE0.2: $Y \approx 0.2 \text{ MPa}$, PLCE0.15: $Y \approx 0.2 \text{ MPa}$, SIS0.01: $Y \approx 0.6 \text{ MPa}$.

B. Nanotube orientation by strain

1. X-ray data analysis

As a crucial part of material characterization, before and during the main actuation experiment, we need a more quantitative analysis of the nanotube orientation in the matrix. It is a key element in our model of the actuation mechanism, but also has its own merit considering the high interest in all aspects of polymer nanocomposite studies. Wide angle X-ray diffraction is used as a method to determine the average tube orientation as a function of increasing applied uniaxial strain. Figure 3(a) shows characteristic features of the diffraction image. The image is for PDMS7, initially non-aligned, stretched by $\epsilon = 0.33$ (33%). The scattering reflection at an angle corresponding to MWCNT [002] layer periodicity (inter-shell spacing [31]) of 3.4\AA allows calculation of the tube orientation distribution from the corresponding azimuthal intensity variation, Fig. 3(b).

In this separate study of deformation-induced alignment we used a 7wt% loaded PDMS7 composite simply to enhance the X-ray contrast and enable using a desktop X-ray generator (as opposed to the synchrotron study required for very low-loading composites). Note that the scattering intensity at 3.4\AA is still relatively low, because of the small contrast between the nanotubes and PDMS matrix.

A question must arise about the bright scattering ring corresponding to the length scale $\sim 7.5\text{\AA}$. This is a very interesting feature, but totally irrelevant for our work: this scattering is exactly the same in the pristine PDMS rubber prepared in the same batch. In the PDMS network, with no solvent, the only X-ray contrast may arise due to the difference between the chains and crosslinks. A very clear scattering length must be an indication of crosslink density fluctuations (in other terminology called clustering). As the extensive theory of this clustering phenomenon suggests [32], at the given chain lengths and crosslinking density the network is well below the ‘crosslink saturation threshold’ and the correlation length of clustering should be of the order of network mesh size. The length scale of $\sim 7.5\text{\AA}$ is very accurately this size and, accordingly, we believe this scattering to be produced by very small scale crosslink density fluctuations. These should not affect macroscopic properties, or even the local MWCNT embedding.

Intensity variation along the azimuthal arcs, $I(\beta)$ in Fig. 3(b), is the signature of the orientational distribution function. When $I(\beta)$ is approximated as a Legendre polynomial series in $\cos \beta$, it gives a measure of the orientational order parameter S_d :

$$S_d \equiv \langle P_2 \rangle = \frac{3}{2}(\langle \cos^2 \beta \rangle - 1), \quad (1)$$

where the averaging is performed with $I(\beta)$ as the distribution function. This is called the Herman’s orientation parameter and it adequately describes the true orienta-

tional ordering at very small bias, when $S_d \ll 1$.

At higher degree of alignment (such as, for instance, in nematic liquid crystals) the orientational distribution function significantly deviates from the measured $I(\beta)$. The analytic treatment of the problem of X-ray scattering from orientationally biased medium is developed by Deutsch [29], mainly in the context of nematic liquid crystals. Instead of using the full theory, we have derived an interpolating analytical approximation to the complete results of [29]. With that, the orientational order parameter is given by

$$S_d = 1 - \frac{3}{2N} \int_0^{\pi/2} I(\beta) \sin \beta \left\{ \sin \beta + \cos^2 \beta \ln \left[\frac{1 + \sin \beta}{\cos \beta} \right] \right\} d\beta \quad (2)$$

$$\text{with } N = \int_0^{\pi/2} I(\beta) d\beta.$$

This expression also properly accounts for nontrivial geometric factors involved in projecting the 3D orientational distribution onto a 2D detector plane. Experimental data was analyzed using both Herman’s approximation and Deutsch’s interpolated analytic result. We conclude that in the range of parameters we are working with both expressions were in agreement qualitatively but slightly differ quantitatively. We favor the Deutsch analytical method and used it exclusively in this study.

2. Induced orientation of nanotubes

Figure 5 presents the results of the calculation of orientational order parameter S_d , acquired as a function of sample strain applied to the PDMS7 sample, as well as the prediction of the theoretical model discussed below. As the applied strain is increased, the initially disordered nanotubes align along the strain axis resulting in bias in the azimuthal curve $I(\beta)$. This phenomenon has recently been confirmed by synchrotron experiments [33] although it should be noted that the focus of the work by Kelarakis *et al.* was not on nanotube reorientation in a rubbery matrix. Our composites, with no significant initial alignment, on subsequent stretching reached substantial values of induced orientational order. Furthermore, the change in orientation on stretching was reversible, i.e. equilibrium, which is discussed later. To our knowledge, this is the first time nanotube *reorientation* has been reported and analyzed in a semisolid/rubberly sample.

As will be described in section IV, there is good evidence that much better nanotube alignment can be achieved if dispersed in a monodomain liquid crystal elastomer during processing – the mesogenic moieties act to align the tubes. A similar effect has been demonstrated for pure liquid crystals [34, 35], and also is well-known in

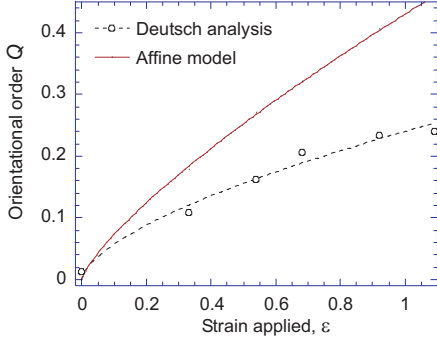


FIG. 5: The change in the orientational order parameter S_d of nanotubes in PDMS7 composite, as a function of imposed uniaxial strain, obtained from the X-ray scattering data (o - data points; dashed line is a guide to the eye). Solid line shows the affine rigid rod model prediction.

the field of ferromematics [36]. X-ray diffraction of such a system is not reported due to the continuing problem of poor contrast between the two species and only low nanotube concentrations studied.

There is an issue, well argued in the literature [37, 38], about whether a truly isotropic nanotube dispersion can be obtained. Regarding the tubes as rigid rods with extremely high aspect ratio, well dispersed in an amorphous medium, the Onsager transition to the steric orientational ordering could start at very low concentrations as has been recently reported [39]. We have as yet observed no clear indication of truly nematic liquid crystalline architecture in our system, although this could be due to a number of factors including matrix viscosity and sample preparation.

3. Affine model of induced orientation

Let us compare the observed induced orientational order parameter $Q(\varepsilon)$ with a simple model prediction based on the affine deformation of the rubbery matrix. The most straightforward approach is to evaluate the average orientational bias resulting from an imposed uniaxial extension of such a matrix, in which the ensemble of rigid rods is initially embedded isotropically. The direction, known as the director \mathbf{n} , is the average axis along which nanotubes can and do align. This is a local property of the system obtained as a result of averaging of individual particle axes, \mathbf{u}_i , over the macroscopically infinitesimal volume. This averaging applies equally well for rigid rod-like particles and for the segments of semi-flexible chains, e.g. in the study of nematic polymers [4]. The corresponding local orientational order parameter is a second-rank tensor $Q_{\alpha\beta}$ which for the uniaxial alignment (reflecting the quadrupolar symmetry breaking) is

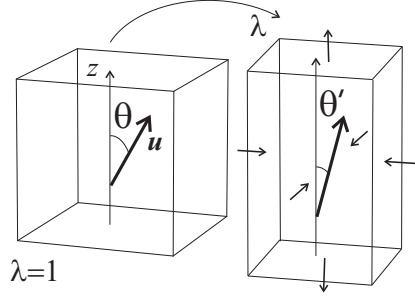


FIG. 6: The scheme of an affine incompressible extension, changing the orientation of an inflexible rod embedded in the medium.

defined as:

$$Q_{\alpha\beta} \equiv \frac{3}{2}Q(n_\alpha n_\beta - \frac{1}{3}\delta_{\alpha\beta}) \equiv \begin{pmatrix} -\frac{1}{2}Q & 0 & 0 \\ 0 & -\frac{1}{2}Q & 0 \\ 0 & 0 & Q \end{pmatrix}, \quad (3)$$

where the principal axes are aligned with z along the uniform ordering direction \mathbf{n} , cf. Fig. 6. The value of the local scalar order parameter is indeed the average of the second Legendre polynomial of orientation of embedded rods,

$$Q \equiv S_d = \int_0^\pi [\frac{3}{2} \cos^2 \theta - \frac{1}{2}] P(\theta) \sin \theta d\theta d\varphi. \quad (4)$$

Here $(\mathbf{n} \cdot \mathbf{u}_i) \equiv \cos \theta_i$ for each rod, and $P(\theta)$ is the orientational probability distribution, normalized such that $\int P(\theta) \sin \theta d\theta d\varphi = 1$. Let us assume the initial state is un-aligned, and thus characterized by the flat distribution $P_0(\theta) = 1/(4\pi)$.

The uniaxial extension of an incompressible elastic body is described by the matrix of strain tensor

$$\boldsymbol{\Lambda} = \begin{pmatrix} 1/\sqrt{\lambda} & 0 & 0 \\ 0 & 1/\sqrt{\lambda} & 0 \\ 0 & 0 & \lambda \end{pmatrix}, \quad (5)$$

where the axis of stretching is taken as z and the magnitude of stretching is $\lambda = 1 + \varepsilon \equiv L/L_0$ is the ratio of the stretched and the initial sample length along z , Fig. 6. This tensor describes the affine change of shape, which could also be visualized as locally transforming an embedded sphere (representing the orientational distribution P_0) into the ellipsoid (representing the induced orientational bias) of the same volume and the aspect ratio $R_{\parallel}/R_{\perp} = \lambda^{3/2}$.

After such a deformation, every element of length in the body changes affinely according to the matrix product $\mathbf{L}' = \boldsymbol{\Lambda} \cdot \mathbf{L}$, which in our case of uniaxial incompressible extension means that $L'_z = \lambda L_z$ and $L'_{\perp} = (1/\sqrt{\lambda})L_{\perp}$. This corresponds to the new angle of the rod, θ' such that $\tan \theta' = L'_{\perp}/L'_z = (1/\lambda^{3/2}) \tan \theta$. Therefore, to obtain the new (now biased) orientational distribution

function we need to convert the variable θ into the new (current) variable θ' , which gives (after some algebraic manipulation)

$$\begin{aligned}\theta &\rightarrow \arctan(\lambda^{3/2} \tan \theta'); \\ \sin \theta d\theta &\rightarrow \frac{\lambda^3}{(\cos^2 \theta' + \lambda^3 \sin^2 \theta')^{3/2}} \sin \theta' d\theta'.\end{aligned}\quad (6)$$

This defines the expression for the normalized orientational distribution function

$$P(\theta') = \frac{\lambda^3}{4\pi(\cos^2 \theta' + \lambda^3 \sin^2 \theta')^{3/2}}, \quad (7)$$

which is an explicit function of the uniaxial strain applied to the body and can be used to calculate the induced order parameter Q :

$$Q(\varepsilon) = \frac{3}{2} \int \frac{\cos^2 \theta' [1 + \varepsilon]^3 \sin \theta' d\theta' d\varphi}{4\pi(\cos^2 \theta' + [1 + \varepsilon]^3 \sin^2 \theta')^{3/2}} - \frac{1}{2}. \quad (8)$$

Analytical integration of this expression gives a function $Q(\varepsilon)$, which is plotted as a solid line in Fig. 5:

$$\begin{aligned}Q(\varepsilon) &= \frac{3 + 2\varepsilon(3 + 3\varepsilon + \varepsilon^2)}{2\varepsilon(3 + 3\varepsilon + \varepsilon^2)} \\ &+ \frac{3(1 + 2\varepsilon(3 + 3\varepsilon + \varepsilon^2))^3}{4\varepsilon(3 + 3\varepsilon + \varepsilon^2)\sqrt{1 - (1 + \varepsilon)^3}} \ln B(\varepsilon)\end{aligned}$$

$$\text{where } B(\varepsilon) = \left[\frac{-1 + (1 + \varepsilon)^3 + \sqrt{1 - (1 + \varepsilon)^3}}{1 - (1 + \varepsilon)^3 + \sqrt{1 - (1 + \varepsilon)^3}} \right].$$

At relatively small strains, it approaches the linear regime: $Q \approx \frac{3}{5}\varepsilon - \frac{6}{35}\varepsilon^2 + \dots$

The experimental data displays a lower order parameter than that predicted by the affine model, although has the same qualitative trend. One must remember that the model presented here does not account for tube flexibility. Also, some proportion of the tubes would be unable to orientate affinely due to the entanglements. The experimental data reflects this and, accordingly, gives slightly lower values of order parameter.

IV. INFRARED ACTUATION

A. Typical observations

The detailed response to infrared stimuli is presented in Figs. 7, showing the stress measured in the PDMS1 sample. Results for all composites are qualitatively similar. We shall later examine the dependence on the host polymer and the tube concentration. Composites, initially un-aligned, are subjected to an increasing extension that we call pre-strain ε . At each ε , the IR-irradiation takes place and the stress response recorded. The complexity of the plots necessitates more detailed description of what takes place.

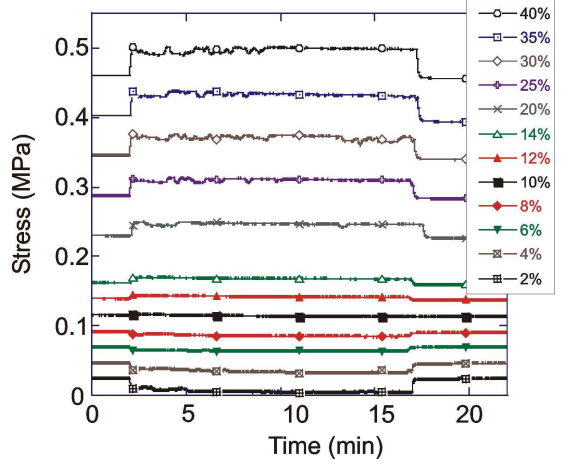


FIG. 7: The response of a 1wt% nanocomposite PDMS1 to IR radiation at different levels of pre-strain ε . Stress is measured at fixed sample length (different pre-strain curves labelled on the plot).

We begin with a 2% pre-strain ($\varepsilon = 0.02$) applied to it initially. At $t = 2$ mins the light source is switched on and the stress reading changes downwards, meaning that the sample natural length L_0 has expanded on actuation (recall that the actual length L is fixed through $\varepsilon = L/L_0 - 1$). After a period of constant irradiation, at $t = 15$ mins, the light source is switched off – and the stress reading returns to its original value. This experiment is then repeated with the same sample pre-strained at different values, up to 40%, as shown by the sequence of stress-reading curves in Fig. 7.

The data in Fig. 8 is assembled to demonstrate the speed of the actuation process more clearly, while Fig. 9 helps differentiate between the light- and heat-driven actuation response. In this case the data is for a PDMS3 composite; as was mentioned above, all materials exhibit the same qualitative features. We plot the change in stress and change in temperature, normalized by their maximal value at saturation in the given experiment; plotted in this form, all the results (for different tube loading and different pre-strain) appear universal.

The change in temperature by IR-heating is unavoidable and reaches $\Delta T \sim 15^\circ\text{C}$ maximally on the sample surface, in our setting (thermocouples placed below the surface and embedded in the center of the sample may report the temperature change of up to 20°C depending on nanotube concentration, but we avoided disturbing the sample in mechanical experiments). This highlights an important question as to whether the mechanical response is due to the photon absorption or plain heat. Figure 9 shows that the stress reaches its peak and saturation in ~ 0.5 min, while the thermal takes over 2min to reach its peak. Although the difference in rates is not very dramatic, the fact that the stress response is faster suggests that its mechanism is not caused by the trivial sample heating. In a separate study (not shown) we reach

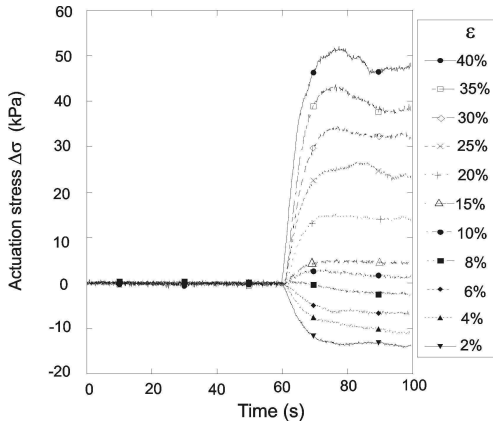


FIG. 8: The speed of actuation response, illustrated by plotting the actuation stress in PDMS3 nanocomposite, $\Delta\sigma$ in kPa, as a function of time for different pre-strain values (labelled on the plot).

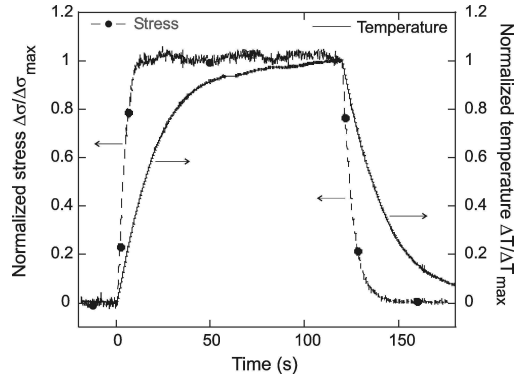


FIG. 9: The normalized stress response plotted alongside the normalized change in temperature, as functions of time (PDMS3, pre-strain $\varepsilon = 20\%$), see text for discussion.

the conclusion that thermo-mechanical effects do exist (i.e. the MWCNT-loaded composite has a stronger mechanical response to heating than a pristine polymer) but their magnitude is almost an order of magnitude smaller than the direct IR-photon absorption mechanism.

B. Analysis of IR-actuation response

Of great interest is the observation that this response changes sign at a certain level of pre-strain (at $\varepsilon \sim 10\%$ in Fig. 7). In other words, relaxed or weakly stretched composites show the reversible *expansion* on irradiation, while the same sample, once strained more significantly, demonstrates an increasing tendency to *contract* (hence the increase in the measured stress). This is our key finding.

Figure 10 summarizes the magnitude of the IR-actuation effect by plotting the stress step at saturation ($\Delta\sigma_{\max}$) in the IR-on state, at different levels of pre-strain and for samples with increasing MWCNT loading.

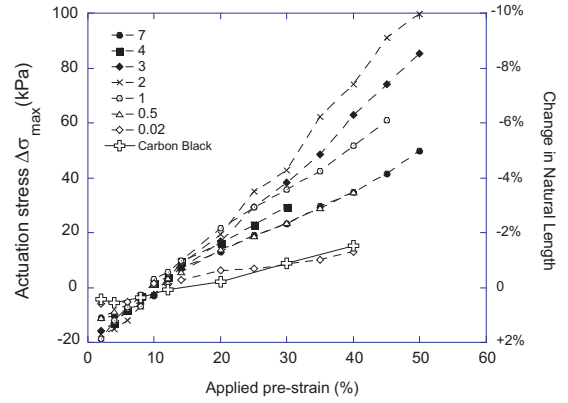


FIG. 10: The magnitude (in kPa) of exerted actuation stress (the height of steps in Fig. 7, $\Delta\sigma_{\max}$), as function of pre-strain. Different PDMS composites are labelled on the plot by their wt% value. The right y -axis shows the corresponding actuation stroke: the change in natural length $L_0(\text{IR})$.

Although this is not explicitly measured in our (isostain, $L = \text{const}$) experiment, we can directly calculate the change of the underlying natural length $L_0(\text{IR})$ of the samples on actuation from the known Young modulus values. This is shown on the right axis of the same plot, highlighting the regions of expansion and contraction. Remarkably, all samples with different nanotube loading appear to have a crossover at the same point, around 10% pre-strain.

For comparison, the pristine PDMS rubber in the same experiment, shows no discernible stress response at all. Also, the response of the PDMS composite with a 3wt% of carbon black is much lower. Indeed, this 3wt% carbon-black composite closely follows the low-concentration PDMS0.02 composite. We believe the response is due to trace amounts of nanotubes that can often be found in commercially supplied carbon black. Hence the very small response from such a highly loaded sample. The shift in transition pre-strain may well be due to the trace nanotubes having their alignment hindered by the activated carbon black.

The interaction between filler particles is also evident when the nanotube concentration is increased beyond 2wt% loading. Above this value, the magnitude of the actuation stroke decreases sharply. Figure 11 displays the effect clearly by plotting the maximal change in natural length L_0 on IR irradiation, at a fixed $\varepsilon = 40\%$, for all PDMS-nanotube composites, and the 3wt% carbon black system for comparison. A rapid increase in the stroke is observed with increasing concentration, which then peaks at 2wt% nanotube loading. The reason for the subsequent decline is not obvious. There may well be a number of factors that interplay to reduce the stroke magnitude. At high concentrations entanglements between the long tubes could take place. Note that through conservation of volume, a contraction in the z -axis of the tube will be concomitant with an expansion in the x - y plane; such expansion may be hindered for a significant

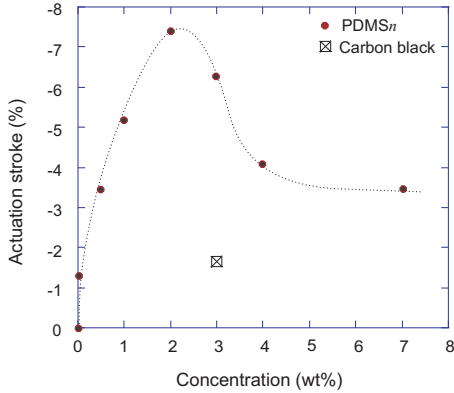


FIG. 11: The magnitude of the actuation stroke at $\varepsilon = 40\%$ as a function of filler concentration n . The maximum of the response at $\sim 2\text{wt\%}$ is evident. The single square symbol gives the value for 3wt% carbon black filler in PDMS.

number of nanotubes by their nearest neighbors (another representation of entanglement). There may also be an issue of photon screening at higher concentration which is difficult to avoid.

C. Observations in other host polymers

Other polymers acting as a crosslinked host matrix for the low-concentration nanocomposite display the same qualitative behavior as PDMS systems. Figure 12 summarizes the response of LCE and SIS composites. The direction of the actuation, changing from expansive to contractive mode with increasing MWCNT alignment, as observed in PDMS-nanotube samples, is unambiguously reproduced for vastly different materials.

The magnitude of the actuation stroke is shown in Fig. 12, in comparison with some of the PDMS composites. The value of actuation stress is different for various polymeric systems considered in this work, which is due to the different Young modulus (which we use to calculate the stroke from the measured stress $\Delta\sigma$). We see that the stroke magnitude in these differing materials is in the same range of magnitudes. SIS0.01 has a much lower filler concentration, and again its stroke is comparable to that of a similarly loaded PDMS0.02. This important finding demonstrates the universality of multi-walled nanotubes behaving as photo-actuators regardless of the soft matrix they are in.

The response of nematic liquid crystal elastomers to heat is well documented [4]. Because they can be thermo-responsive materials, the data in Fig. 12 is obtained by a complex procedure of subtraction of such background effects. We do not go into its details, as this is irrelevant to the main points of the present paper, however, must emphasize that the plotted response highlights the effect of nanotubes within the given matrix.

In Fig. 12 we note that the MLCE0.2 sample shows

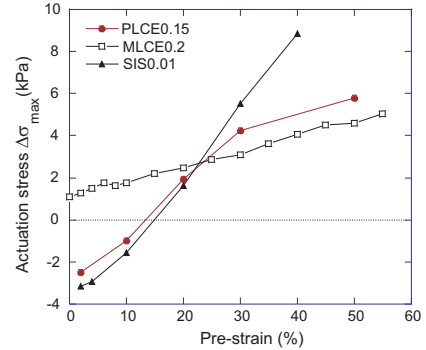


FIG. 12: Summary of IR actuation stroke from LCE composites (PLCE0.15 and MLCE0.2) and a SIS0.1 composite, as a function of applied pre-strain. Note that MLCE data does not have a crossover at $\varepsilon \sim 10\%$, since the tubes are aligned there at preparation. For comparison, the similar data for two PDMS samples, 0.5 and 0.02, is shown by dashed lines.

no expansive actuation and a crossover, while the similar polydomain (un-aligned) composite does. This is clearly because the two-step crosslinking at preparation of the monodomain material involves aligning the mesogenic groups [27]. The embedded nanotubes align strongly under such conditions, as others have found in ordinary liquid nematics [34, 35]. As already discussed, the expansive mode of actuation will only occur when the degree of nanotube alignment is very low. It is important that the crossover occurs at $\varepsilon^* \sim 10\%$ for all studied materials with nanotubes not aligned before pre-strain.

V. MODELLING THE MECHANISM

There are two main questions to answer: what mechanism is responsible for such a large photo-mechanical response, and why does it reverse its direction on sample extension?

We shall try to deduce the actuation behavior of individual tubes from the macroscopic observations detailed above. We believe the change of actuation direction on increasing sample extension is due to the nanotube alignment induced by pre-strain, as described in section III B and before. In the whole region of our pre-strains, the orientational order induced in the MWCNT distribution is, to a good approximation, a linear function of the strain: $S_d \approx 0.6\varepsilon$ in the affine model. At the crossover strain $\varepsilon^* \approx 0.1$, the value of the order parameter would be $S_d^* \sim 0.06$. We now apply the same ideas about the induced orientational bias and averaging of the (hypothetical) individual nanotube response.

Let us assume this individual nanotube response to the IR photon absorbtion is, in essence, a contraction – because this is what our data shows the better-aligned composite response to be. It is easy to imagine why this could be for an initially rod-like tube: on photon absorbtion it could generate instabilities in the form of kinks,

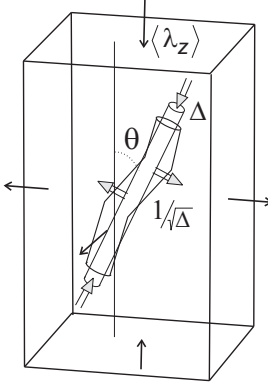


FIG. 13: The scheme illustrating how the distortion (kinking) of an individual tube, lying at an angle θ to the macroscopic alignment axis, projects on the z -axis to contribute to the average uniaxial strain, Eq. (10).

thus decreasing the net length due to the charge carrier separation. The resulting elastic deformation would be most pronounced in the already defect-dominated regions of the nanotube. Such an explanation, based on concentration of induced polarons [40, 41], would also link with the earlier observation of a similar actuation response under DC electric field [24]. An alternative possibility is to suggest that large (and fast) local tube heating [42] causes the surrounding region of locally aligned elastomer to contract and “crush” the nanotube. This version of microscopic events does not contradict the discussion and the data in Fig. 9, which shows the (slow) global thermal effect.

At this stage we have to leave open the question of individual tube response to near IR radiation. Using an affine approach similar to the earlier analysis of ordering, let us assume that each nanotube undergoes a linear contraction by a factor $\Delta = R_{\parallel}(\text{IR})/R_{\parallel}(0) < 1$ (certainly proportional to radiation intensity, which was kept constant in our work but has previously been shown to effect the elastic response [19]). This contraction must be accompanied by a transversely-isotropic volume conserving expansion $1/\sqrt{\Delta}$. This means that a local strain is created with the principal axes along the nanotube orientation (at angle θ to the macroscopic z -axis, see Fig. 13)

$$\Lambda_{\text{local}} = \begin{pmatrix} 1/\sqrt{\Delta} & 0 & 0 \\ 0 & 1/\sqrt{\Delta} & 0 \\ 0 & 0 & \Delta \end{pmatrix}.$$

The projection of this local strain on the macroscopic axis of sample extension (and force measurement) is

$$\lambda_z(\text{IR}) = \Delta \cos^2 \theta + (1/\sqrt{\Delta}) \sin^2 \theta. \quad (9)$$

Averaging the local contribution with the probability to find the nanotube at this orientation, $P(\theta)$ obtained in section III B, gives an estimate of the effective stroke of

the actuation. When multiplied by the corresponding Young modulus, the exerted stress of Fig. 10 is also obtained: $\Delta\sigma = Y(\langle\lambda_z\rangle - 1)$ at small deformations. Such a model is very crude indeed, ignoring a large number of undoubtedly important and delicate factors of continuum elasticity and nanotube response. However, it is elastically self-consistent and has only one parameter, Δ that presumably carries all the underlying complexity of the problem in it.

The orientational averaging is given by using the distribution $P(\theta)$ with the projection of local strain in Eq. (9):

$$\begin{aligned} \langle\lambda_z\rangle &= \int_0^\pi [\Delta \cos^2 \theta + (1/\sqrt{\Delta}) \sin^2 \theta] P(\theta) \sin \theta d\theta d\varphi \\ &\approx \frac{1}{3} (\Delta + 2/\sqrt{\Delta}) - \frac{2}{5} \varepsilon (1/\sqrt{\Delta} - \Delta) \end{aligned} \quad (10)$$

Although the integral above has a full analytic form, it is more transparent to present its expansion to the linear order of small imposed pre-strain ε as shown in the second line of Eq.(10). This demonstrates the key point: at very low pre-strain, $\varepsilon \rightarrow 0$, the average uniaxial deformation of the disordered nanocomposite is positive ($\lambda_z - 1$), i.e. the expansion of its natural length. However, above a threshold pre-strain ε^* this average deformations transforms into the sample contraction along z . It is easy to find the crossover,

$$\varepsilon^* \approx \frac{5(2 - \Delta^{1/2} - \Delta)}{6(1 + \Delta^{1/2} + \Delta)}, \quad (11)$$

so that the prediction would be to observe the crossover at $\varepsilon^* \sim 0.1$ if the nanotube response factor $\Delta \sim 0.8$. That is, on IR-irradiation the nanotube contracts overall by $\sim 20\%$. The value is higher than one might expect, considering early reports in the literature of nanotube strains of only 1-2%. However, as Fig. 13 indicates, our proposition is not that of the lattice strain of nanotube walls but a contortion of the tube as a whole. Although this has not been yet directly observed and reported in the literature, a similar effect of resonant undulation has been seen (in simulation [43] and in experiment [16]) in response to distortion beyond the linear regime. Furthermore, the more recent theoretical work on single-walled tubes supports the idea that massive z -axis contraction. Although in our system the multi-walled tubes respond under different conditions, being embedded in an elastic matrix under strain and absorbing the IR photons, the overall distortion factor of 20% suggested by the model fit is perhaps not altogether unreasonable.

Figure 14 plots the full (non-expanded) result of orientational averaging of actuation stroke ($\langle\lambda_z\rangle - 1$) from the integral in Eq.(10) to illustrate the points discussed in this section. The qualitative behavior (as summarized in Fig. 10) is reproduced here almost exactly, including the magnitude of the predicted actuation stroke [that is, the ratio $L_0(\text{IR})/L_0(0) - 1$]. Note that we use only one parameter, Δ to match both the crossover ε^* and the actuation stroke magnitude, so the conclusion is quite satisfac-

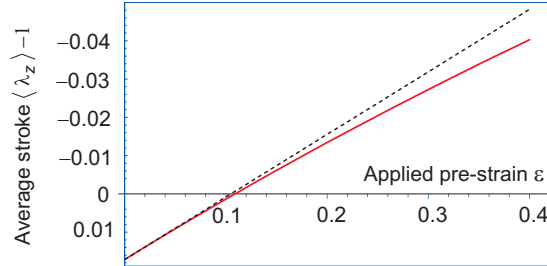


FIG. 14: The result of the affine theoretical model, Eq. (10); the dashed line shows the linear approximation at small pre-strain. Nanotube contraction factor is chosen to be $\Delta = 0.8$, as suggested by the crossover strain value $\varepsilon^* \sim 0.1$.

tory and agrees with an apparent universality discussed in section IV C. It is very likely that the orientational feature of the effect, with its change of actuation direction at a critical level of induced alignment, $S_d \sim 0.06$, is captioned correctly, while much more work is required to understand the individual nanotube response to IR radiation generating the phenomenological factor Δ used in this analysis.

VI. CONCLUSIONS

To summarize, this work describes the rich photo-actuation phenomena of carbon nanotubes embedded in crosslinked rubbery matrices. The composite materials show the ability to change their actuation direction, from expansive to contractive response, as greater imposed strain is applied to the sample. We use differing host polymers and confirm their relatively neutral role in the actuation mechanism.

Theoretical models have been put forward to describe the orientational order imposed on the nanotubes by a uniaxial strain and the resulting actuation. Treating the nanotubes as rigid rods that rotate affinely in a deforming matrix is a very simplistic view, but it gives predictions that agree with experiment qualitatively and often quantitatively. We believe that the (certainly wrong) idea of the whole tube acting as a rigid rod is not actually nec-

essary – in effect, in our model, the “rigid rods” are nanotube segments below persistence length. In that case, as in main-chain semiflexible nematic polymers, the model is non-controversial and the agreement with experiment not coincidental. The tube orientational distribution appears to account well for the key macroscopic features of the observed photo-actuation.

The strength of photo-mechanical response, at a given radiation intensity, is of the order of tens of kPa. Translated into the stroke, this corresponds to actuation strains of +2 (expansion) to -10% (contraction) depending on the nanotube concentration, alignment (controlled by pre-applied strain) and the host matrix. As expected, the response increases at higher nanotube loading – however, only up to a limit. Beyond this limit ($\sim 2\%$ in PDMS), the macroscopic actuation is inhibited by inter-tube interactions and possible charge accumulation. The similar (thermal actuation) behavior is also observed when the samples are heated by the same amount, but this has a much lower amplitude.

Understanding the nature of the actuator mechanisms in this system certainly warrants further theoretical and experimental investigation. Many questions remain completely unclear, in particular, what the effect would be if different types of nanotube were used i.e. smaller multi-wall diameters, single-wall tubes, various chirality etc. With actuating materials already used in such widespread applications, from micromanipulators to vibration control, the discovery of a structure that can respond to stimulus in both directions may open new possibilities and could mean an important new step toward finding applications for nanotube based materials above and beyond improvements in existing carbon fibre technologies.

Acknowledgments

We thank H. Körner, R. Vaia, A. Craig and P. Cicuta for useful discussions, and K. Channon for help with nanotube absorbance data. This work was carried out with the support of the Engineering and Physical Sciences Research Council and a CASE award from Makevale Ltd.

-
- [1] J. E. Huber, N. A. Fleck, and M. F. Ashby, Proc. Roy. Soc. London Ser. A. **453**, 2185 (1997).
 - [2] K. Bhattacharya, *Microstructure of Martensite*, Oxford University Press, Oxford, 2004.
 - [3] A. Lendlein, A. Schmidt, and R. Langer, Proc. Nat. Acad. Sci. **98**, 842 (2001).
 - [4] M. Warner and E. M. Terentjev, *Liquid Crystal Elastomers*, Oxford University Press, Oxford, 2003.
 - [5] S. V. Ahir and E. M. Terentjev, Nature Mater. **4**, 491 (2005).
 - [6] N. W. S. Kam, M. O'Connel, J. A. Wisdom, and H. J. Dai, Proc. Nat. Acad. Sci. **102**, 11600 (2005).
 - [7] P. M. Ajayan and T. W. Ebbesen, Rep. Prog. Phys. **60**, 1025 (1997).
 - [8] L. Forro and C. Schonenberger, *Physical properties of multi-wall nanotubes*, vol. 80 of *Topics in Applied Physics*, 2001.
 - [9] R. Saito, G. Dresselhaus, and M. S. Dresselhaus, *Physical properties of carbon nanotubes*, Imperial College Press, London, 1998.
 - [10] O. Breuer and U. Sundararaj, Polym. Comp. **25**, 630 (2004).
 - [11] R. Andrews and M. C. Weisenberger, Curr. Opin. Solid State Mater. Sci. **8**, 31 (2004).

- [12] P. J. F. Harris, Int. Mater. Rev. **49**, 31 (2004).
- [13] E. T. Thostenson, Z. F. Ren, and T. W. Chou, Comp. Sci. Technol. **61**, 1899 (2001).
- [14] S. V. Ahir and E. M. Terentjev, in: *Polymeric Nanosstructures and Their Applications*, American Scientific Publishers, ed H.S. Nalwa (2006)
- [15] J. Cumings and A. Zettl, Science **289**, 602 (2000).
- [16] P. Poncharal, Z. L. Wang, D. Ugarte, and W. A. de Heer, Science **283**, 1513 (1999).
- [17] P. A. Williams, S. J. Papadakis, A. M. Patel, M. Falvo, S. Washburn and R. Superfine, Phys. Rev. Lett. **89**, 255502 (2002).
- [18] A. Fennimore, T. D. Yuzvinsky, W. Q. Han, M. S. Fuhrer, J. Cumings and A. Zettl, Nature **424**, 408 (2003).
- [19] Y. Zhang and S. Iijima, Phys. Rev. Lett. **82**, 3472 (1999).
- [20] B. J. Landi, R. P. Raffaelle, M. J. Heben, J. L. Alleman, W. VanDerveer and T. Gennett, Nano Lett. **2**, 1329 (2002).
- [21] H. Koerner, G. Price, N. A. Pearce, M. Alexander, and R. A. Vaia, Nature Mater. **3**, 115 (2004).
- [22] M. Tahhan, V. T. Truong, G. M. Spinks, and G. G. Wallace, Smart Mater. Struct. **12**, 626 (2003).
- [23] J. Naciri, A. Srinivasan, H. Jeon, N. Nikolov, P. Keller and B. R. Ratna, Macromolecules **36**, 8499 (2003).
- [24] S. Courty, J. Mine, A. R. Tajbakhsh, and E. M. Terentjev, Europhys. Lett. **64**, 654 (2003).
- [25] A. Garg and S. B. Sinnott, Chem. Phys. Lett. **295**, 273 (2002).
- [26] S. B. Sinnott, J. Nanosci. Nanotechnol. **2**, 113 (2002).
- [27] J. K  pfer and H. Finkelmann, Macromol. Chem.-Rapid Comm. **12**, 717 (1991).
- [28] Papers in:, *Developments in Block Copolymers*, Applied Science Publishers Ltd, Oxford, ed I. Goodman (1982).
- [29] M. Deutsch, Phys. Rev. A **44**, 8264 (1991).
- [30] R. E. Gorga and R. E. Cohen, J. Polym. Sci. B-Polym. Phys. **42**, 2690 (2004).
- [31] J. C. Charlier and J. P. Michenaud, Phys. Rev. Lett. **70**, 1858 (1993).
- [32] S. Panyukov and Y. Rabin, Phys. Rep. **269**, 1 (1996).
- [33] A. Kelarakis, K. W. Yoon, I. Sics, R. H. Somani, B. S. Hsiao and B. Chu, Polymer **46** (2005).
- [34] M. Lynch and D. Patrick, Nano Lett. **97**, 1197 (2002).
- [35] I. Dierking, G. Scalia, P. Morales, and D. LeClere, Adv. Mater. **16**, 865 (2004).
- [36] S. Burylov and Y. Raikher, Phys. Rev. E **50**, 358 (2004).
- [37] A. M. Somoza, C. Sagui, and C. Roland, Phys. Rev. B **6308**, 081403 (2001).
- [38] M. F. Islam, A. M. Alsayed, Z. Dogic, J. Zhang, T. C. Lubensky and A. G. Yodh, Phys. Rev. Lett. **92**, 088303 (2004).
- [39] W. H. Song and A. H. Windle, Macromolecules **38**, 6181 (2005).
- [40] M. Verissimo-Alves, R. B. Capaz, B. Koiller, E. Artacho, and H. Chacham, Phys. Rev. Lett. **86**, 3372 (2001).
- [41] V. Perebeinos, J. Tersoff, and P. Avouris, Phys. Rev. Lett. **94**, 086802 (2005).
- [42] P. M. Ajayan and M. Terrones and A. de la Guardia and V. Huc and N. Grobert and B. Q. Wei and H. Lezec and G. Ramanath and T. W. Ebbesen, Science **296**, 5568 (2002).
- [43] B. I. Yakobson, C. J. Brabec, and J. Bernholc, Phys. Rev. Lett. **76**, 2511 (1996).